Conformation and Dynamics of Atactic Poly(acrylonitrile). 3. Characterization of Local Structure by Two-Dimensional $^{2}H-^{13}C$ Solid-State NMR

Hironori Kaji*,†,‡ and Klaus Schmidt-Rohr‡,§

Department of Polymer Science and Engineering, University of Massachusetts, Amherst, Massachusetts 01003, Institute for Chemical Research, Kyoto University, Uji, Kyoto, 611-0011, Japan, and Department of Chemistry and Ames Laboratory, Iowa State University, Ames, Iowa 50011

Received April 16, 2001; Revised Manuscript Received July 5, 2001

ABSTRACT: The detailed conformational structure of a disordered crystalline polymer, atactic poly(acrylonitrile) (aPAN), has been characterized by two-dimensional (2D) NMR experiments. A solid-state $^{2}H-^{13}C$ heteronuclear multiple-quantum correlation (HMQC) NMR experiment has been applied to an aPAN sample containing both α-hydrogen-deuterated and $^{13}C{\equiv}N$-carbon-labeled repeat units. The 2D spectrum yields information in particular on the two successive torsion angles in racemo trans−trans dyads. Their average values are found as (180 ± 5°, 180 ± 5°), with distributions of standard deviation $\sigma = 10 \pm 5°$ for both torsion angles. The torsion angles and their distributions in racemo trans−trans dyads thus obtained are closer to the ideal trans conformation than are those in meso trans−trans dyads determined by 2D double-quantum solid-state NMR spectroscopy on a $^{13}C{\equiv}N$-carbon-labeled aPAN sample. The differences are considered to originate from larger steric hindrance and larger electric dipole interaction between the C≡N groups in meso trans−trans dyads. The experimental spectra are also compared with those calculated for three models for PAN proposed in the literature. Further detailed analyses of the 2D spectra and their projections have also yielded information on intermolecular side group alignments. There are indications that the $^{13}C{\equiv}N$ side groups are oriented preferentially along the crystalline lattice directions *a*, *b*, and $-(a + b)$ in the hexagonal lattice. Intermolecular antiparallel alignments of C≡N groups, often found in organic nitrile compounds, have not been observed in the 2D spectra.

1. Introduction

In our preceding papers,[1,2] the trans:gauche ratio and the detailed torsion angles in meso dyads in atactic poly(acrylonitrile) (aPAN) were investigated, by homonuclear two-dimensional (2D) double-quantum (DQ) solid-state nuclear magnetic resonance (NMR) spectroscopy[3,4] (DOQSY).[5] This method was applied to a 15% $^{13}CH_2$-carbon-labeled aPAN ($^{13}CH_2$-aPAN) sample and to a 100% ^{13}CN-carbon-labeled aPAN (^{13}CN-aPAN). These experiments revealed that the trans:gauche ratio in aPAN is 90%:10% (±5%). The average torsion angles and their distributions in meso trans−trans (*mTT*) dyads were found to deviate by 10−20° from the ideal trans conformation, with a wide distribution of standard deviation $\sigma = 20 \pm 5°$. Typical average torsion angles are (+160 ± 10°, +160 ± 10°) and/or (±170 ± 5°, ∓170 ± 5°).

This dyad-specific analysis was possible because the *mTT* and racemo trans−trans (*rTT*) dyads give very different DOQSY powder patterns for ^{13}CN-aPAN, due to the different relative orientations of adjacent $^{13}C{\equiv}N$ groups. Thus, in principle this experiment could also give quantitative torsion angle information for racemo dyads. In practice, however, the analysis is not so straightforward. First, the DQ excitation efficiency for *rTT* dyads is weak.[2] Second, DOQSY patterns of *rTT* dyads overlap those of gauche-containing meso dyads due to geometric similarities. Third, the *rTT* dyad signals also overlap with those of intermolecular correlations, which cannot be neglected, because a 100% ^{13}CN-carbon-labeled aPAN sample was used to obtain a good signal-to-noise ratio. Thus, a new approach is necessary to determine the torsion angles of *rTT* dyads precisely.

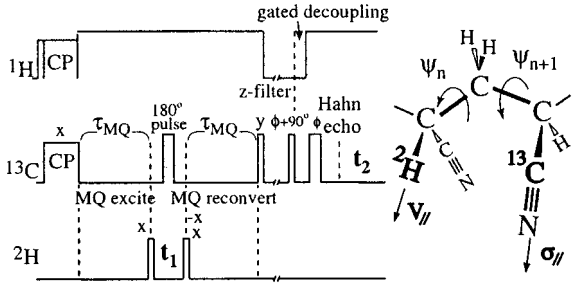

Figure 1. Pulse sequence and schematic representation of the solid-state $^{2}H-^{13}C$ HMQC 2D experiment, which correlates the orientation-dependent ^{2}H quadrupolar coupling of an α-deuteron along ω_1 with the ^{13}C chemical shift anisotropy of a neighboring ^{13}CN group along ω_2.

In this paper, average torsion angles and their distributions in *rTT* dyads of aPAN are characterized by a solid-state $^{2}H-^{13}C$ 2D heteronuclear multiple-quantum (MQ) correlation (HMQC) experiment. The experiment is performed on a statistical copolymer of 75% α-hydrogen-deuterated and 25% $^{13}C{\equiv}N$-carbon-labeled acrylonitrile ($^{2}H/^{13}CN$-aPAN) (Figure 1). This experiment can provide torsion angles with excellent accuracy, because the chemical shift tensor orientation of $^{13}C{\equiv}N$ carbons and the electric field gradient tensor

* To whom correspondence should be addressed at Kyoto University. E-mail: kaji@molmat.kuicr.kyoto-u.ac.jp.
† Kyoto University.
‡ University of Massachusetts.
§ Iowa State University.

10.1021/ma010658c CCC: $20.00
Published on Web 09/13/2001

orientation of $C-^2H$ deuterons are well-defined. The axially symmetric chemical shift anisotropy (CSA) of the $^{13}C\equiv N$ carbons and the quadrupolar coupling of the α-deuterons probe specific $C\equiv N$ triple-bond and $C-^2H$ single-bond directions, respectively. In the ^2H dimension, the coupling strength is much larger than the ^{13}C CSA, and dipolar splittings by the ^{14}N nucleus[2] are unobservable; therefore, the $^2H-^{13}C$ correlation is expected to yield even better angular resolution than the 2D DOQSY ^{13}C NMR experiments.

In the *rTT* dyads, the $^2H-^{13}C\equiv N$ correlation spectrum of the $-C^2H(-C\equiv N)-CH_2-CH(-^{13}C\equiv N)-$ sequences gives signals near the diagonals; the distances between the ^2H and ^{13}C nuclei are mostly shorter than in meso dyads, and MQ generation is more efficient. This experiment is complementary to 2D DOQSY of ^{13}CN-aPAN and gives detailed information on *rTT* dyads of aPAN. It is therefore concluded that the torsion angles of meso and racemo dyads, including their distributions, can be determined specifically by the combination of the above-mentioned 2D ^{13}C DOQSY and 2D $^2H-^{13}C$ HMQC experiments. To our knowledge, this is the first quantitative study of dyad-specific conformational information directly in an atactic polymer. The results obtained are also compared quantitatively with models of aPAN conformations that have been proposed in the literature. In addition, intermolecular correlations are explored.

2. Experimental Section

2.1. Samples. A powdered 75% 2-^2H/25% 1-^{13}C-labeled aPAN ($^2H/^{13}CN$-aPAN) sample was polymerized from a mixture of [2-^2H]acrylonitrile and [1-^{13}C]acrylonitrile at a ratio of 75:25. The details of the polymerization procedure, processing, and characterization of the polymerized sample are described in our previous paper.[1] The viscosity average molecular weight is 1.2×10^5, and the triad tacticity measured by solution ^{13}C NMR is *mm*:*mr*:*rr* = 29:50:21. The wide-angle X-ray diffraction (WAXD) pattern showed the pseudohexagonal chain packing, which is the most commonly reported polymorph.

2.2. NMR Measurements. The solid-state NMR experiments were performed on a Bruker DSX-300 spectrometer in a static magnetic field of 7 T. The isotropic $^2H/^{13}CN$-aPAN powder sample was inserted as a cylindrical block into a 4.2 mm diameter coil of a Bruker triple-resonance CP/MAS probe. The measurements were carried out at 298 K without sample rotation. Cosine data sets were measured on-resonance in ω_1 and processed to yield purely absorptive, nonquadrature spectra. Since the phase structure of aPAN is not well understood yet,[6] we measured all the components in aPAN, without using any filters for the selection of certain morphological components. For a detailed discussion on the phase structure of aPAN, see ref 1. The pulse sequence for 2D $^2H-^{13}C$ HMQC experiments to be applied to $^2H/^{13}CN$-aPAN is shown in Figure 1. The ^1H and ^{13}C 90° pulse lengths were 4.0 and 2.9 μs, respectively. ^2H pulses flanking the t_1 evolution time were 1.5 μs, which correspond to approximately 45° flip angles, reducing pulse-excitation distortions in the ^2H dimension. A cross-polarization time of 2 ms, a recycle delay of 8 s, a *z*-filter before detection of 2 ms, an acquisition time of 3.12 ms, a dwell time of 6 μs, and ^1H decoupling fields $\gamma\mathbf{B}_1/2\pi$ of 66 kHz were used. The pulses were applied at a frequency near the center of the spectrum. The τ delay for the Hahn echo was 22 μs. During the Hahn echo, ^1H decoupling was turned off for 20 μs to dephase the signal of natural-abundance aliphatic ^{13}C directly bonded to ^1H. Note that the magnetization of ^{13}C nuclei directly bonded to ^2H is not dephased. Two spectra with the MQ excitation and reconversion delays, $\tau_{MQ} = 0.45$ ms and 0.8 ms, were added up. For the experiment with $\tau_{MQ} = 0.45$ ms, 64 t_1 slices with increments of 1 μs were acquired with 160 scans per slice. For the experiment with $\tau_{MQ} = 0.8$ ms, 72 t_1 slices with increments of 1 μs were acquired with 128−256 scans per slice. The total acquisition time was 57 h. Linear backward prediction by 3 μs was carried out for the t_1 dimension to reproduce the ^2H Pake pattern for the sum spectrum in the ω_1 dimension.

3. NMR Background

3.1. Angle-Dependent NMR Frequencies. The NMR frequency reflects the orientation of a given molecular unit relative to the external magnetic field $\mathbf{B}_0$. Both for carbons in $-^{13}C\equiv N$ groups and deuterons in aliphatic $-C-^2H$ groups, the chemical shift tensor and the electric field gradient tensor are uniaxial, and their unique principal axes are directed along the $-^{13}C\equiv N$ and $-C-^2H$ bonds, respectively, as shown in Figure 1. The NMR frequency is then described as[7]

$$\omega_{aniso}(\theta) = \pm\frac{\delta_{aniso}}{2}(3\cos^2\theta - 1) \qquad (1)$$

where θ is the angle between the $-^{13}C\equiv N$ or $-C-^2H$ bond and the $\mathbf{B}_0$ field directions. The + and − signs in eq 1 apply only to ^2H NMR, where they correspond to the two transitions allowed for the spin-1 nucleus. In the following, the orientation-dependent frequencies, ω_{aniso}, appear as ω_S and ω_Q for $-^{13}C\equiv N$ carbons and $-C-^2H$ deuterons, respectively.

3.2. $^2H-^{13}C$ 2D HMQC Experiment. Here, we briefly describe the principle of the solid-state version of $^2H-^{13}C$ HMQC experiments.[8−10] The pulse sequence as applied to the $^2H/^{13}CN$-aPAN sample is shown in Figure 1. We consider a pair of four-bond-separated ^2H and ^{13}C nuclei with quadrupolar frequency ω_Q and chemical shift ω_S, respectively. The Hamiltonian of the heteronuclear dipolar coupling between S = ^{13}C and L = ^2H spins is denoted by H_D^{SL}. When we consider the pulse sequence in Figure 1, the separation of the initial S_x density operator into two components

$$S_x = S_x(\mathbf{1} - L_z^2) + S_xL_z^2 \qquad (2)$$

makes the calculation simpler. Since the first term in eq 2 is invariant under the action of the heteronuclear Hamiltonian, H_D^{SL}, we need to consider the second term only. The second term, $S_xL_z^2$, evolves during the pulse sequence "(MQ excitation)−(90° L_x)−(t_1 evolution)−(90° $L_{\mp x}$)−(MQ reconversion)" as follows, focusing only on the relevant terms in the density operator:

$$\begin{aligned}
\text{MQ excitation:}\quad & S_xL_z^2 \xrightarrow{H_D^{SL}\tau_{MQ}} S_yL_z\sin(2\omega_{SL}\tau_{MQ}) \\
& \xrightarrow{(\pi/2)L_x} S_yL_y\sin(2\omega_{SL}\tau_{MQ}) \\
\text{t}_1\text{ evolution:}\quad & \xrightarrow{\omega_Qt_1L_z^2} S_yL_y\sin(2\omega_{SL}\tau_{MQ})\cos(\omega_Qt_1) \qquad (3) \\
& \xrightarrow{(\pi/2)L_{\mp x}} \pm S_yL_z\sin(2\omega_{SL}\tau_{MQ})\cos(\omega_Qt_1) \\
\text{MQ reconvert:}\quad & \xrightarrow{H_D^{SL}\tau_{MQ}} \mp S_xL_z^2\sin^2(2\omega_{SL}\tau_{MQ}) \\
& \qquad\qquad \cos(\omega_Qt_1)
\end{aligned}$$

Here we have considered only the heteronuclear (SL) dipolar and ^2H quadrupolar couplings of frequencies ω_{SL}

and ω_Q, respectively. The chemical shift of the S nucleus during the period between MQ excitation and MQ reconversion is totally refocused by the π pulse in the middle of this period. After a *z*-filter, S_y-related components, which are not described in eq 3, have decayed by transverse (T_2) relaxation. Additional terms, such as cosine components in the MQ excitation and reconversion periods, as well as the first term in eq 2, exist even after the *z*-filter. However, they are subtracted by appropriate phase cycling. Thus, the observable during the acquisition period becomes (per scan)

subtraction by phase cycling:

$$\rightarrow S_x {L_z}^2 \sin^2(2\omega_{SL}\tau_{MQ}) \cos(\omega_Q t_1) \quad (4)$$

This is observed as a modulation of the ^{13}C signal in the detection period t_2. The 2D time domain signal is thus

$$S(t_1,t_2) = {g_{het}}^2(\tau_{MQ})\left(\frac{2}{3}\right)\cos(\omega_Q t_1)\exp(i\omega_S t_2) \quad (5)$$

where

$$g_{het}(\tau_{MQ}) = \sin(2\omega_{SL}\tau_{MQ}) \quad (6)$$

The $\sin(\omega_Q t_1)$ data set cannot be detected in a similar way. For the experiment, only the cosine data set was measured and processed to yield purely absorptive, symmetric ^{2}H spectra.

Equations 5 and 6 show that the 2D ^{2}H−^{13}C HMQC spectrum, which correlates the orientation-dependent frequencies ω_Q in the first dimension and ω_S in the second dimension, is obtained with the intensity weighted by ${g_{het}}^2(\tau_{MQ})$, which depends on the ^{2}H−^{13}C dipolar coupling strength.

4. Results and Discussion

4.1. ^{2}H−^{13}C 2D HMQC Simulation. Figure 2 shows simulated ^{2}H−^{13}C 2D HMQC spectra of ^{2}H/^{13}CN-aPAN for some typical torsion angles. The dyad configuration (meso or racemo) and two successive backbone torsion angles intervening between C−^{2}H and ^{13}CN sites are specified above each spectrum. The two successive backbone bonds are not equivalent in the ^{2}H−^{13}C correlation experiments, while they can be interchanged without altering the 2D DOQSY patterns for the ^{13}CN-aPAN sample.[2] Throughout this paper, we will use the convention that the first torsion angle refers to the ^{2}HC−CH$_2$ bond and the second to the CH$_2$−CH(^{13}CN) bond. In this experiment, we do not need to consider the ^{14}N spin−lattice relaxation effect on the 2D patterns since the triplet splitting due to ^{14}N only affects the directly bonded ^{13}C, during the detection period. Thus, only three patterns with different ^{13}C CSA principal values are added up for the simulated spectra.

The spectra in Figure 2a−d demonstrate that the HMQC experiment provides high angular resolution; the conformations with $rT'\bar{T}'$ (+170°, −170°), $r\bar{T}'T'$ (−170°, +170°), and $rT'T'$ (+170°, +170°) can be distinguished from rTT (180°, 180°). The rTT conformations, Figure 2a, give 2D patterns that are characteristically different from those of the mTT and mTG conformations, Figure 2e,i. In contrast, in the homonuclear 2D DOQSY experiments, rTT and mTG conformations produce similar patterns (see Figure 4 in ref 2). In addition, TG and GT conformations give different 2D HMQC spectra, while they are equivalent in 2D DOQSY experiments. The mGT conformations (not shown) give similar straight-ridge patterns as the rTT conformations due to geometric equivalence, but since we know that the content of mGT is small,[1,2] the contribution of the rTT conformation must be dominant. Thus, the ^{2}H−^{13}C 2D HMQC experiment reveals the conformation of racemo dyads.

4.2. Experimental ^{2}H−^{13}C 2D HMQC Spectrum. Figure 3a shows the experimental ^{2}H−^{13}C 2D HMQC spectrum of ^{2}H/^{13}CN-aPAN. The ^{2}H quadrupolar splitting, ω_Q, in the ω_1 dimension is correlated with the ^{13}C CSA, ω_S, in ω_2. The feature of the rTT dyads is observed in the widest splittings of ∼240 kHz in the ω_1 dimension at −30 to −120 ppm in the ω_2 dimension. The features of mTT (or mTG) are observed in the ridges parallel to the ω_2 axis, with an ω_1 splitting of ∼120 kHz, and in the splittings wider than 120 kHz at 250−150 ppm. In addition to these features, significant intensities are observed in the splittings of ∼120 kHz at about 60, 20, and −20 ppm. These originate mainly from C−H carbons directly bonded to ^{2}H; note that their signal does not decay during gated decoupling. The C−^{2}H carbon resonance lines should be triplets with equal intensities due to the dipolar interaction with ^{2}H. However, the central intensity is higher than the others in the experimental spectrum, indicating the existence of residual CH$_2$ signals. In the following simulations, these aliphatic signals are also included.

The finite pulse width effect for ^{2}H is also considered in the simulations, by multiplying the following excitation function onto the intensity along the ω_1 dimension, for each of the two pulses on ^{2}H:[7,11,12]

$$X(\omega_1) = \omega_{B1} t_p \frac{\sin(\omega_{eff} t_p)}{\omega_{eff} t_p} \quad (7)$$

Here, t_p is the ^{2}H pulse width, $\omega_{B1} = \gamma B_1$, and ω_{eff} is given by

$$\omega_{eff}(\omega_1) = \left({\omega_{B1}}^2 + \frac{1}{4}{\omega_1}^2\right)^{1/2} \quad (8)$$

where ω_1 is the ^{2}H quadrupolar "frequency offset".

4.3. Comparison of Experimental and Simulated ^{2}H−^{13}C 2D HMQC Spectra. Parts b−i of Figure 3 show simulated spectra of ^{2}H/^{13}CN-aPAN with various average torsion angles and torsion angle distributions. The contributions of mTT, mTG, mGT, and rTT including aliphatic signals are superimposed in the simulations. In each spectrum, the weight is (mTT + mTG + mGT):rTT = 54:46 and mTT:mTG:mGT = 34:10:10, which gives a trans content of 90%. Similarly as for the homonuclear 2D DOQSY spectra in the preceding paper in this issue,[2] the parameter set ($\bar{\psi}_n$, ψ_{n+1}; σ) is used for the description of the averages of two successive torsion angles (ψ_n, ψ_{n+1}) and the standard deviation σ of the Gaussian distribution of torsion angles. The Gaussian distributions for both torsion angles are presumed to have the same σ. Dyads in which the distance between the relevant two ^{13}C sites in a pair of ^{13}CN groups is smaller than 2.52 Å were excluded (see ref 2). The torsion angle increment used in the simulations was 5°. The discussion here is focused on the conformation of racemo dyads. For the mTT dyads, on the basis of the result of our preceding DOQSY study,[2] a conformation of (+160°, +160°; σ = 20°) is used in the simulations of Figure 3b−h. For mTG and mGT dyads, the parameter sets (+170°, +70°; σ = 10°) and

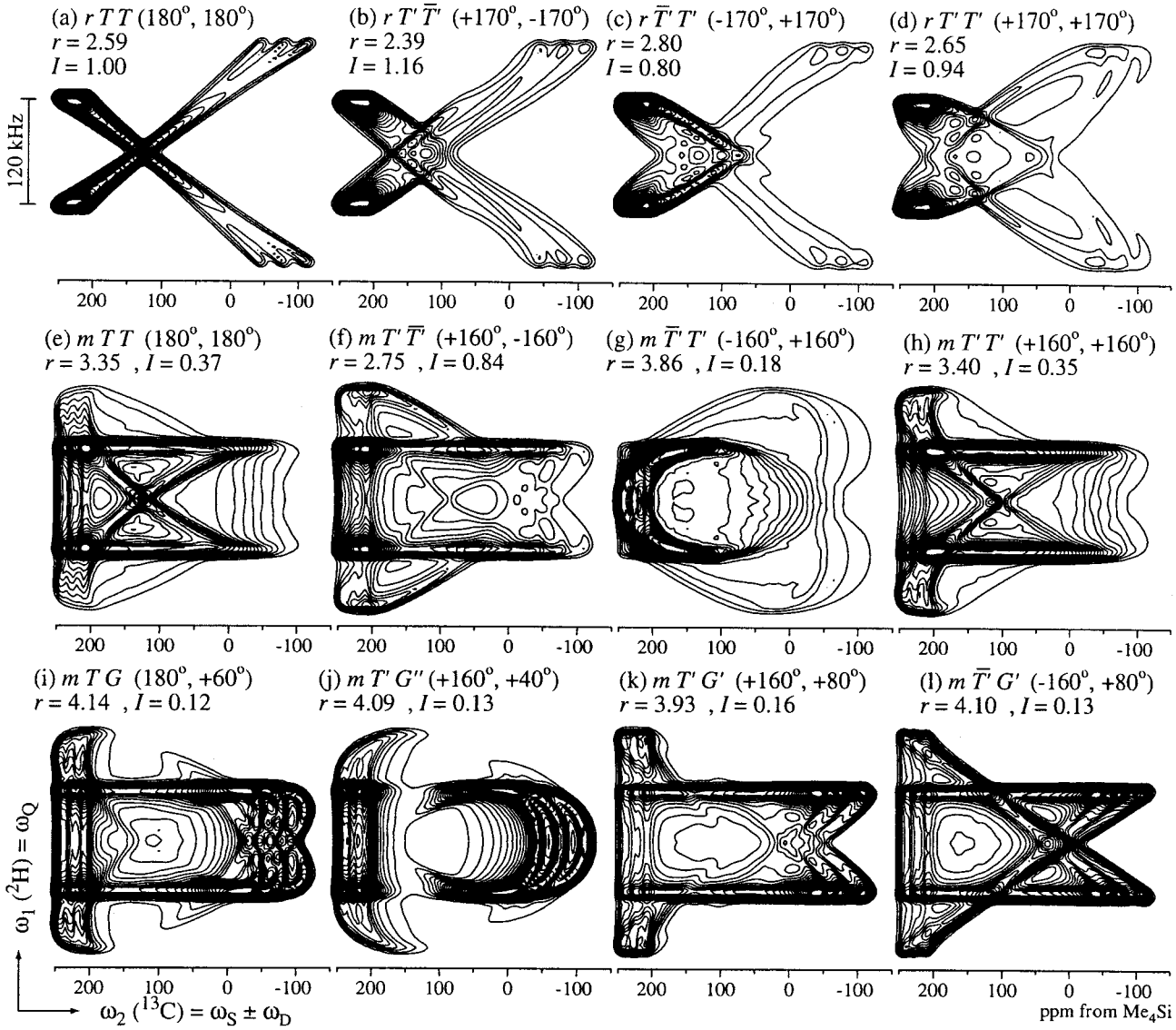

Figure 2. Simulated $^2H-^{13}C$ 2D HMQC spectra of $^2H/^{13}CN$-aPAN for typical conformations. The dyad configurations and two successive torsion angles are indicated above each spectrum. The $^2H-^{13}C$ distances, *r*, between the two relevant $-C-^2H$ deuterons and C≡N carbons, and the volume intensities, *I*, relative to the exact *rTT* state are also given. Parameters used for the simulations are as follows: $\angle C^\alpha-C-C^\alpha = 113°$ for meso dyads and 111° for racemo dyads, $\angle C-C^\alpha-CN = 109.5°$, $r(C-C^\alpha) = 1.54$ Å, $r(C^\alpha-CN) = 1.46$ Å, $r(C^\alpha-H) = 1.09$ Å. The ^2H quadrupolar splitting is 126 kHz, and three spectral patterns with the principal values of ($\sigma_\perp$, $\sigma_\parallel$) = (243, −120), (226, −86), and (209, −52) ppm are superimposed for ω_2. Two simulations with an MQ excitation time of τ_{MQ} = 0.45 and 0.8 ms have been summed up. Gaussian broadenings with standard deviations of 4 kHz and 5 ppm were applied along ω_1 and ω_2, respectively. Thirty contour lines are plotted between 3% and 90% of the maximum intensity.

(+70°, +170°; σ = 10°) are used for all simulations in this figure. The spectra with a single *rTT* conformation, such as (180°, 180°; σ = 0°), (+170°, +170°; σ = 0°), and (+170°, −170°; σ = 0°) + (+170°, −170°; σ = 0°) in Figure 3b−d, show a clear diagonal ridge or elliptical ridges. In the experimental spectrum, these clear ridges are not observed and the diagonal ridge is significantly broadened. This indicates that the torsion angles are distributed even for *rTT* dyads. Note that, for Figure 3d, two conformations should be averaged (summed up and then divided by 2 to yield the correct intensity relative to that of *mTT*, *mTG*, and *mGT*). This is because we have two $^2H-^{13}CN$ pairs in the respective dyads, whose conformations are (ψ_n, ψ_{n+1}) and (ψ_{n+1}, ψ_n), respectively (with the first torsion angle consistently referring to the $^2HC-CH_2$ bond). For the rest of Figure 3, Gaussian distributions of torsion angles are used. Parts e and h of Figure 3 are obtained using Gaussian distributions with σ = 10° and σ = 20°, respectively, for the torsion angles of the *rTT* conformation, with averages of (180°, 180°). It is found that the central part of the 2D spectra in the ω_2 range of 160−60 ppm is a good indicator for the torsion angle distribution of the *rTT* conformations. The Gaussian distribution with σ = 10° nicely reproduces the experimental data, indicating that the standard deviation of the torsion angle distribution is σ = 10° within the experimental error of ±5°. Obvious discrepancies with the experimental spectrum are observed when the center of the distribution deviates by =10° from the exact trans−trans state, as is seen in Figure 3f,g; the *rTT* conformation of (−170°, −170°) gives spectra (not shown) quite similar to those of (+170°, +170°), irrespective of σ. This indicates that the average torsion angle for the *rTT* conformation is 180° within the experimental error of ±5°. In Figure 3i, the distribution of (+170°, −170°; σ = 20°) + (−170°, +170°; σ = 20°) is used for *mTT* dyads instead of (+160°, +160°; σ = 20°).

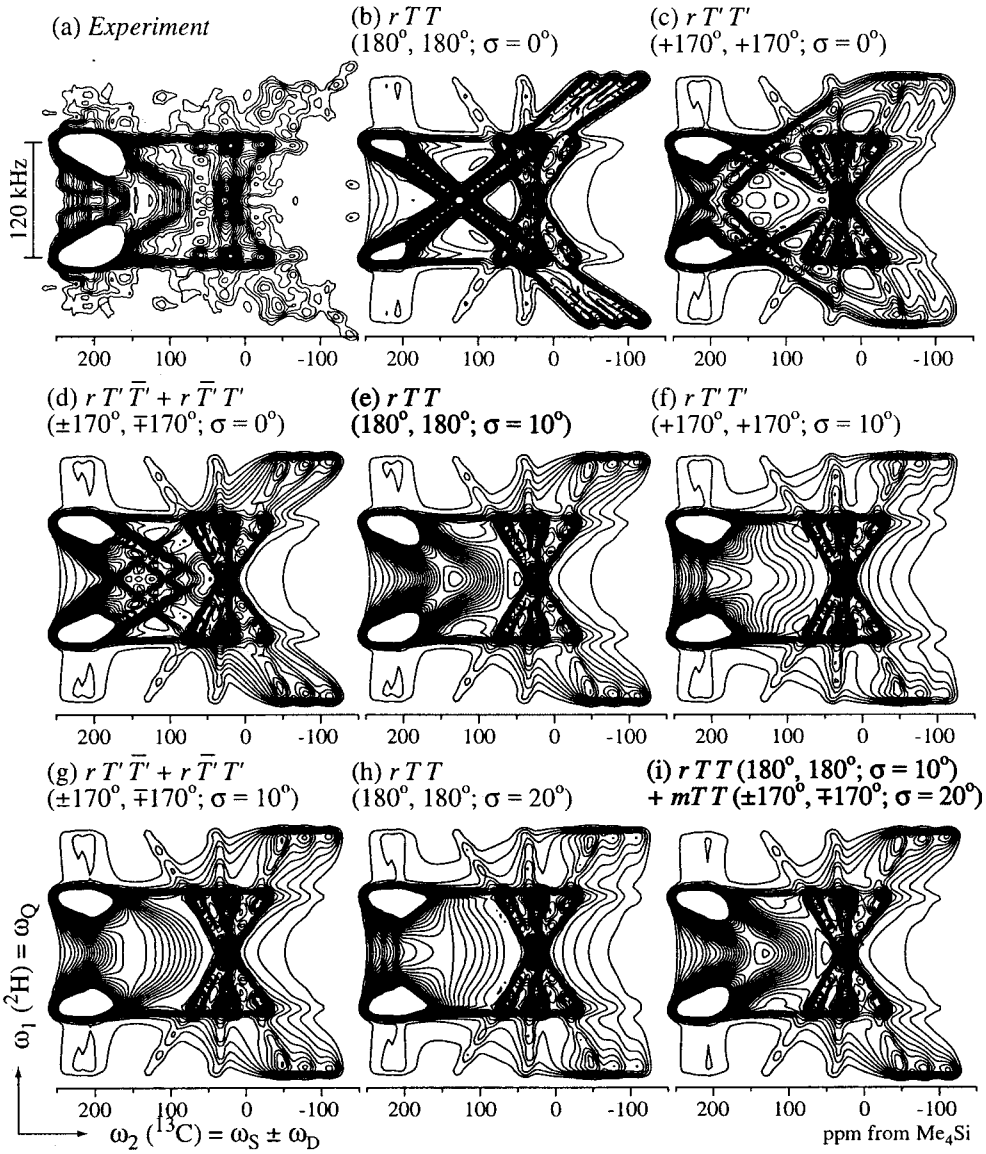

Figure 3. $^2H-^{13}C$ 2D HMQC spectra of $^2H/^{13}CN$-aPAN. Two spectra with $\tau_{MQ} = 0.45$ and 0.8 ms are superimposed for all spectra. (a) Experimental spectrum. (b−i) Simulated spectra with various average torsion angles and their distributions for *rTT* dyads (indicated above each spectrum). Four contributions, *mTT*:*mTG*:*mGT*:*rTT* = 34:10:10:46 (meso:racemo = 54:46 and trans content 90%), are summed up, assuming that the *G* conformers are all part of the *mTG* and *mGT* dyads. Two torsion angle sets that will necessarily occur together have been superimposed for both (d) and (g). Average torsion angles and distribution widths of (+170°, +70°; $\sigma = 10°$) and (+70°, +170°; $\sigma = 10°$) are used for *mTG* and *mGT* conformations, respectively. The *mTT* conformation of (+160°, +160°; $\sigma = 20°$) is used, except for (i) where the sum of (+170°, −170°; $\sigma = 20°$) and (−170°, +170°; $\sigma = 20°$), divided by 2, is used for the *mTT* conformation instead. Aliphatic signals have also been included. The finite pulse width effect is considered in the simulations. Thirty contour lines are plotted between 1% and 30% of the maximum intensity, except for (b) where 60 contour lines are plotted between 1% and 60%. Other parameters are the same as in Figure 2. The spectrum with *rTT* of (−170°, −170°; $\sigma = 10°$) is similar to (f). Simulations (e) and (i) are similar and produce the best fits of the experimental spectrum.

The other parameters are the same as those of Figure 3e. Both simulations give similar spectra, and we cannot distinguish these two *mTT* conformations even by the 2D $^2H-^{13}C$ correlation experiment. This is consistent with the finding in our preceding paper[2] that conformations of (±170°, ∓170°; $\sigma = 20°$) as well as (+160°, +160°; $\sigma = 20°$) are possible in *mTT* dyads.

4.4. Comparison with Previous Investigations. 4.4.1. Simulated Spectra Based on Models from the Literature. In most previous work on the structure of aPAN, only the conformation of the meso dyads was considered as variable, and a single well-defined trans torsion angle was assumed for racemo dyads. We have obtained *rTT* torsion angles in aPAN experimentally for the first time. The average torsion angles in racemo dyads (180°, 180°) obtained here appear reasonable, because the distance between two adjacent carbons in C≡N groups, 3.50 Å, is much longer than in meso dyads of (+160°, +160°) and (±170°, ∓170°), where it is 3.04 and 2.56 Å, respectively. In this section, comparisons are carried out with a conformational model composed of ideal torsion angles and with conformational models calculated on the basis of syndiotactic PAN (sPAN), since neither experimental nor calculated data on the trans zig-zag conformation of racemo dyads of aPAN are available. In Figure 4b, the simulated 2D HMQC spectrum based on a model by Liu and Ruland[13] is shown. Four types of dyads, *mTT*, *mTG*, *mGT*, and *rTT*, are superimposed at a ratio of 34:10:10:46, which results in meso:racemo = 54:46 and trans:gauche = 90:10. The ideal torsion angles, 180° for *T* and +60° for *G*, are used. The diagonal ridges in Figure 4b are sharper than those

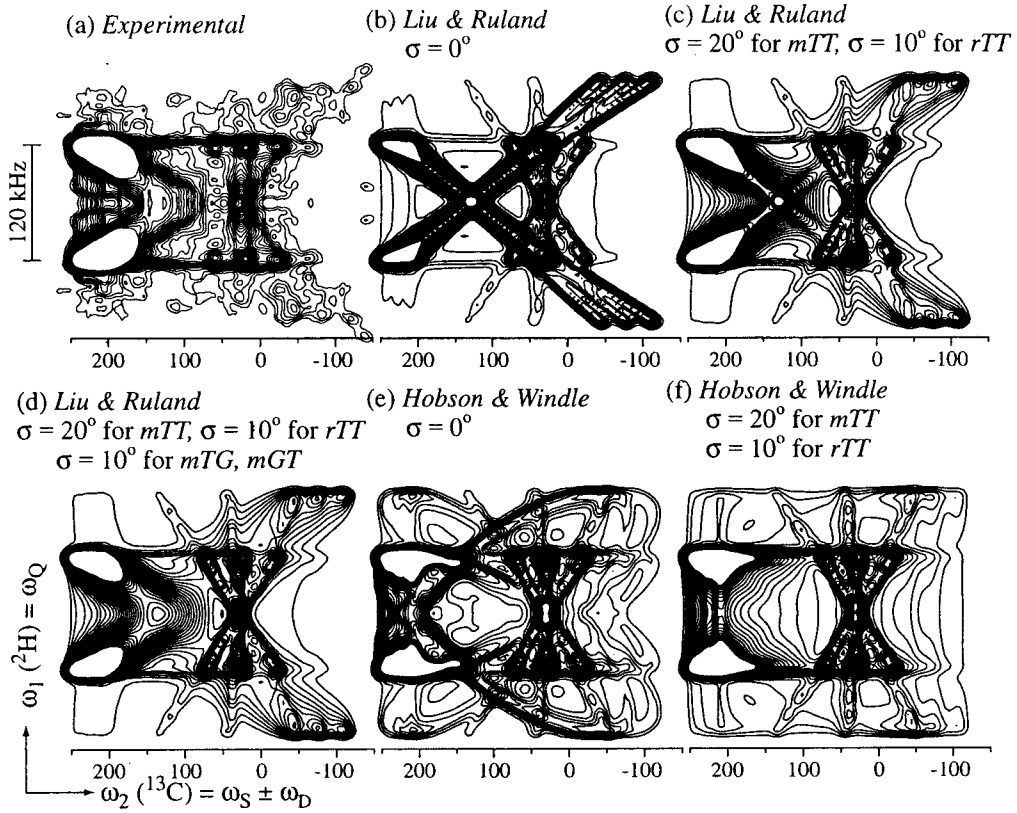

Figure 4. $^2H-^{13}C$ 2D HMQC spectra of $^2H/^{13}CN$-aPAN. Two subspectra with $\tau_{MQ} = 0.45$ and 0.8 ms are superimposed for all spectra. (a) Experimental spectrum. (b–f) Simulated $^2H-^{13}C$ 2D HMQC spectra of $^2H/^{13}CN$-aPAN based on a model by Liu and Ruland (b–d), and on a model by Hobson and Windle (e–f). In (b), four contributions, *mTT*:*mTG*:*mGT*:*rTT* = 34:10:10:46, have been summed up. The "ideal" torsion angles of 180° and +60° are used for *T* and *G*, respectively. In (c), Gaussian distributions with $\sigma = 20°$ and 10° have been applied for *mTT* and *rTT*, while *mTG* and *mGT* still have single well-defined torsion angles. In (d), the torsion angles of *mTG* and *mGT* conformations are also distributed with $\sigma = 10°$. In (e), two contributions, *mTT*:*rTT* = 54:46, have been summed up. The specific torsion angles of (±160°, ∓160°) and (+167°, +167°) are used for *mTT* and *rTT* conformations, respectively. In (f), Gaussian distributions with $\sigma = 20°$ and $\sigma = 10°$ have been applied for *mTT* and *rTT*. Thirty contour lines are plotted between 1% and 30% of the maximum intensity, except for (b). Sixty contour lines are plotted between 1% and 60% for (b). Other parameters are the same as in Figure 3.

in the experimental spectrum, indicating that the torsion angles in *rTT* dyads should be distributed. Therefore, in the spectra of Figure 4c, Gaussian distributions with $\sigma = 20°$ and 10° are applied for the *mTT* and *rTT* dyads, respectively. The diagonal ridges in the spectrum are still sharper than those in the experimental spectrum. The sharper ridges arise from the specific conformation of the *mGT* dyads, which give a pattern similar to that of the *rTT* conformations; see above. It is interesting to note that the *mGT* conformation yields much higher intensity in 2D HMQC than in DOQSY spectra. Thus, even though the content of *mGT* is small,[1,2] the 2D HMQC spectrum can reveal whether the torsion angles in *mGT* dyads have a broad distribution. The absence of sharp diagonal ridges in the experimental spectrum, compared with those of Figure 4c, indicates that the torsion angles in *mGT* dyads have a significant distribution width. Correspondingly, the torsion angles in *mTG* dyads are also expected to be distributed. Therefore, in the spectrum of Figure 4d, Gaussian distributions with $\sigma = 10°$ are applied for the *mTG* and *mGT* dyads. While the resulting spectrum is similar to the experimental spectrum, this does not mean that the torsion angles in meso dyads used in these simulations are proven to be correct; the 2D HMQC spectrum is simply not very sensitive to the torsion angles in meso dyads. The precise torsion angles of *mTT* dyads have been determined previously by a 2D DOQSY experiment on a ^{13}CN-aPAN sample, which is sensitive specifically to the torsion angles of *mTT* dyads.[2]

On the basis of a molecular modeling calculation of oligomers of syndiotactic, i.e., all-racemo, PAN, Hobson and Windle[14] suggest a torsion angle deviation of 13–14° from the exact trans state. The torsion angle of +167° is close to that in syndiotactic polypropylene, 160° or 169°, experimentally determined from a WAXD measurement.[15] Figure 4e shows a simulated 2D HMQC spectrum based on the Hobson and Windle model. They obtained conformations of (±160°, ∓160°) and (+167°, +167°) from isotactic PAN (iPAN) and sPAN oligomer models, respectively, while gauche conformations were not considered. Thus, only two types of dyads, *mTT* and *rTT*, are superimposed at a ratio of 54:46 with conformations of (±160°, ∓160°; $\sigma = 0°$) and (+167°, +167°; $\sigma = 0°$), respectively. The elliptical patterns seen in this simulation are absent from the experimental spectrum in Figure 4a. Even with Gaussian distributions of $\sigma = 20°$ and 10° applied for the *mTT* and *rTT* dyads, respectively, see Figure 4f, the agreement with the experimental spectrum is poor. The introduction of gauche conformations does not improve the fit. It is clear that the inconsistency is due to the 167° torsion angle of the *rTT* dyads. The actual torsion angle in the *rTT* dyads of aPAN found in our experiment is much closer to 180°.

Rizzo et al.[16] also carried out a conformational calculation on sPAN. In their calculation, the torsion angles of sPAN are (±177°, ∓177°). The simulated spectrum based on their model (not shown here) is similar to the experimental spectrum if appropriate distributions are applied for the dyad conformations; Gaussian distributions with $\sigma = 20°$ and 10° for the *mTT* dyads and others, respectively, provide good results. The torsion angle deviation of 3° is found to be below the resolution limit of the present 2D HMQC experiments. However, note that the experimentally determined distribution implies that the torsion angles deviate typically by ±10° from 180°. The ±177° torsion angles, with their slight deviations from 180°, could then be considered as representative conformations.

It is also found that the 2D HMQC spectrum is less sensitive to the trans:gauche ratio than the DOQSY spectrum of aPAN. A trans:gauche ratio of 90:10 determined in our previous papers[1,2] and a trans:gauche:anticlinal ratio of 75:20:5 in Rizzo's model are indistinguishable in the HMQC spectrum.

4.4.2. Torsion Angle Distributions and Phase Structure. The existence of torsion angle distributions for *mTT* dyads and even for *rTT* as well as *mTG* dyads has been revealed by our 2D DOQSY and 2D HMQC spectra. The intermolecular pseudohexagonal packing would force the torsion angle to be distributed to make polymer chains of cylindrical rod shape, with a ca. 5%[16] reduced long period compared to *all-trans*-polyethylene. The conformational distributions revealed in this paper and the preceding paper[2] suggest that aPAN can be considered as a conformationally disordered (condis) phase in Wunderlich's classification,[17,18] as was already suggested in ref 16. Note, however, that the original definition of "condis" refers to a "dynamic" conformationally disordered phase; thus, for aPAN we need to expand the definition to include the case of "static" conformational disorder. It should also be noted that the disorder has a chemical origin, the atactic configuration, rather than a purely entropic reason. For the phase structure, as described in detail in our previous work,[1] there is no direct evidence that indicates the existence of two phases in aPAN. Both homonuclear 2D DOQSY and $^2H-^{13}C$ 2D HMQC spectra can be explained by monomodal Gaussian distributions for each dyad conformer. The high trans content of 90% ± 5% found in the two previous papers in this series leaves little room for a disordered amorphous phase (see also section 4.5.2 of ref 1).

4.5. Origin of Slight Misfit in Best-Fit Simulation, and Intermolecular Correlation. So far, we have given an extensive description of the intramolecular orientational correlations, i.e., between neighboring segments along an aPAN chain. In this section, we consider interchain correlations. This is motivated by slight but possibly significant deviations observed between the experimental DOQSY spectrum of ^{13}CN-aPAN and the corresponding best-fit simulation. This deviation is seen quite clearly in the sum projection spectra shown in Figure 5a,b, which were obtained from the DOQSY spectra of Figure 5a,h of ref 2, respectively. In the DQ sum projections onto ω_1, stronger intensities are observed around 300 ppm as well as between 100 and −100 ppm. We have considered three reasons for the misfit: (i) ^{14}N relaxation effects, (ii) residual signals from aliphatic carbons, and (iii) intermolecular correlations. These will be discussed in the following.

The effect of ^{14}N relaxation (i), neglected in the simulations, will smear out the simulated spectra slightly more, but will not give the above-mentioned additional intensities. (ii) The spectrum of the correlations between C≡N carbons and aliphatic CH and CH_2 carbons has been simulated. The 2D pattern is shown in Figure 6d, and the single-quantum (SQ) and double-quantum (DQ) sum projections are plotted in Figure 5c. Although the 2D spectrum gives intensities between +50 and −50 ppm in ω_2 on the diagonal of slope two, very high signals are observed at the downfield end in ω_1 of the spectrum. It is found that the misfit cannot be explained only by the residual signals from aliphatic carbons.

The spectral effects of intermolecular correlations (iii) depend on the actual packing order in aPAN. We have considered three alternative packing modes. For intermolecular isotropic random C≡N orientations, a simulated 2D DOQSY spectrum and the corresponding sum projections are shown in Figures 6a and 5d, respectively; the simulated $^2H-^{13}C$ 2D HMQC spectrum is displayed in Figure 6e. For random C≡N orientations in the *a*,*b*-plane of the pseudohexagonal crystal lattice of aPAN, the spectra shown in Figures 5e and 6b,f result. Both of these packing models do not give intensities that would account for the misfit.

A third model, with C≡N orientations spaced regularly by 120° in the *a*,*b*-plane, has been considered, see Figures 5f and 6c,g. This model gives intensities in the intended regions as indicated by arrows in Figure 5f. Of course, in reality distributions of C≡N orientations and translational distributions along the chain direction are to be expected. The model is compatible with the calculation in ref 16. The CN directions are nearly perpendicular to the chain axis, and the angles between C≡N groups are 120°. This orients the CN groups along the lattice directions *a*, *b*, and $-(a + b)$ in the hexagonal lattice.

Figure 7 compares the experimental DOQSY and HMQC spectra with simulations that combine the intramolecular and hexagonal intermolecular correlations. The DOQSY simulation of Figure 7b is the sum of 93% of the intramolecular simulation of Figure 5h in ref 2 and 7% of the intermolecular correlation spectrum of Figure 6c. The sum projections of the best-fit spectrum are shown in Figure 5h. They also agree very well with the experimental projections of Figure 5a. In contrast, adding 7% of the intermolecular correlation spectrum (Figure 6b) with random orientations in the *a*,*b*-plane to the intramolecular simulation does not improve the fit. The resulting sum projections, Figure 5g, are not much different from the purely intramolecular simulation.

The HMQC simulation of Figure 7d combines 97% of the intramolecular simulation of Figure 3e with 3% of the intermolecular correlation spectrum of Figure 6g. The intermolecular component is reduced here compared to the $^{13}C-^{13}C$ correlation because the deuteron is closer to the center of the chain. The excellent quality of the DOQSY fit, Figure 7a,b, supports the hypothesis that the intermolecular correlations arise from CN groups pointing approximately along the *a*, *b*, and $-(a + b)$ directions in the crystalline lattice.

The C≡N group has a significant electric dipole moment of 3.9 D,[19] and an antiparallel alignment of two CN groups is observed and theoretically calculated for organic nitriles.[20−24] A deviation from the exact anti-

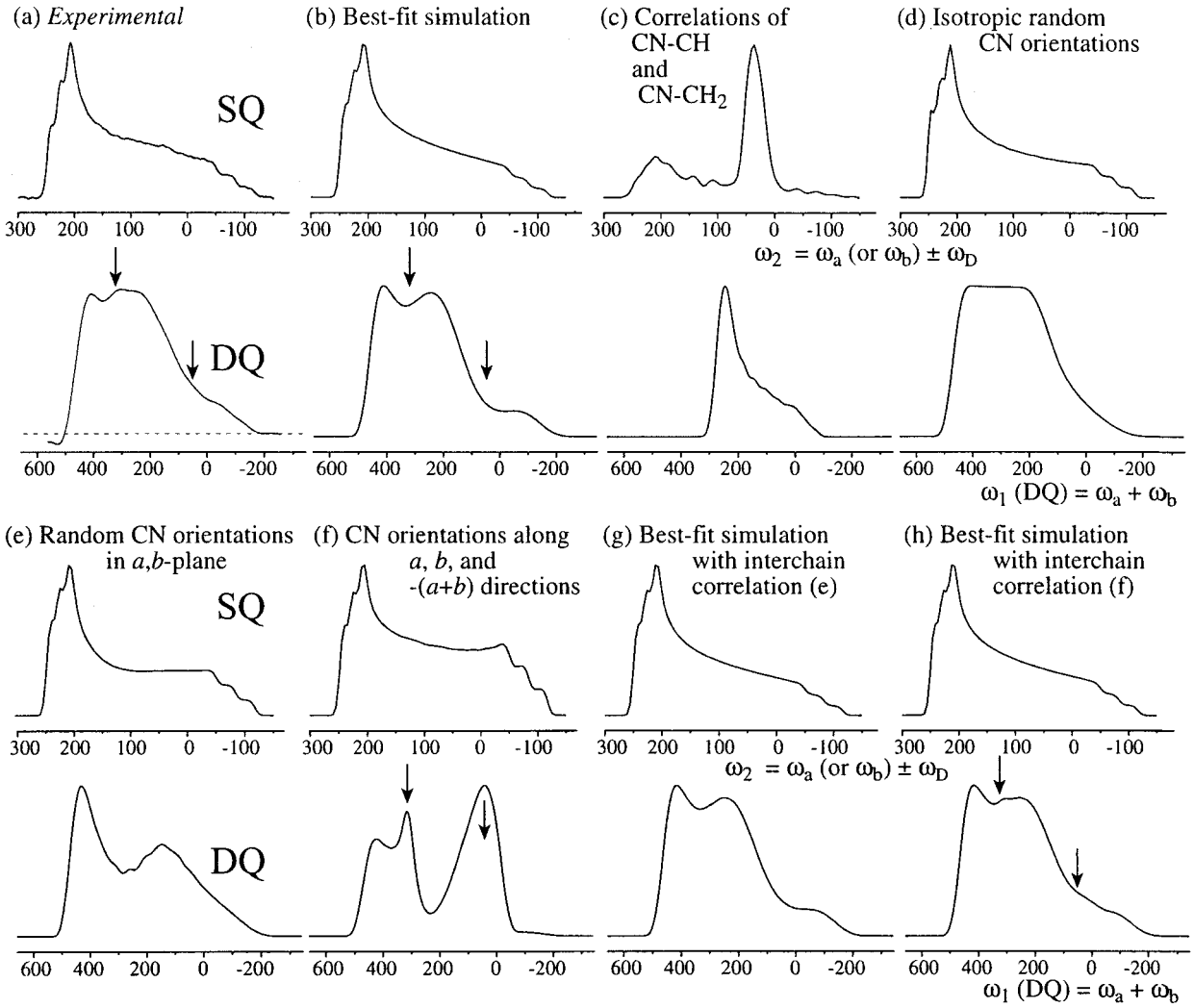

Figure 5. Sum projections of 2D DOQSY spectra onto the ω_2(SQ) and the ω_1(DQ) axes, shown at the top and bottom of each figure, respectively. (a) Experimental spectrum. (b) Best-fit simulated spectrum, which corresponds to the 2D spectrum in Figure 5h in ref 2. (c) Simulated spectra for correlations between $^{13}C{\equiv}N$ and natural-abundance aliphatic carbons, which correspond to the 2D spectrum in Figure 6d. (d–f) Simulated spectra for intermolecular correlations, which correspond to the 2D spectra in Figure 6a–c, respectively. The SQ spectra also depend slightly on the conformation, due to the excitation function $g_{SCL}^2(\tau_{DQ})$; see eq 4 in ref 2. (g) Sum projections of a simulated spectrum combining 93% of the best-fit intramolecular simulation in (b) with 7% of the random in-plane intermolecular correlation spectrum in (e). (h) Sum projections of the best-fit spectrum combining 93% of the best-fit intramolecular simulation in (b) with 7% of the hexagonal intermolecular correlation spectrum in (f). The corresponding 2D DOQSY pattern is shown in Figure 7b.

parallel alignment is energetically unfavorable. We would expect sharp intensities along the diagonal of slope two in the 2D DOQSY spectrum of ^{13}CN-aPAN if there was an intermolecular antiparallel pairing of $C{\equiv}N$ groups. However, such a sharp diagonal ridge of slope two is not observed in the experimental spectrum. Therefore, we must conclude that the amount of intermolecular CN pairing in aPAN is negligibly small despite the large dipole moment of CN groups.

Intermolecular $C{\equiv}N$ correlations, such as parallel alignments or relative orientations of 120° in the *a,b*-plane (see Figure 6), can also be investigated more directly in an aPAN sample that is a homogeneous blend of $C{\equiv}^{15}N$-nitrogen-labeled and $^{13}C{\equiv}N$-carbon-labeled chains. For this purpose, the pulse sequence in Figure 1, but with pulses at the ^{15}N instead of ^2H frequency, was applied to a 2:1 mixture of 100% $C{\equiv}^{15}N$-nitrogen-labeled aPAN and statistically 25% $^{13}C{\equiv}N$-carbon-labeled aPAN ($C^{15}N$-aPAN/^{13}CN-aPAN). Unfortunately, in an experiment with $\tau_{MQ} = 0.5$ ms, we only detected the correlation between the enriched $C{\equiv}^{15}N$ nitrogen and the directly bonded natural-abundance ^{13}C, which is efficiently excited due to the short C–N distance in the $C{\equiv}N$ triple bond. An experiment with longer τ_{MQ} is expected to give the intermolecular information, but we could not use a much longer τ_{MQ} due to fast T_2 relaxation. We plan to measure this correlation with longer distances by utilizing ^1H spin diffusion.

5. Conclusions

We have investigated the quantitative backbone conformation of racemo dyads in aPAN in its disordered crystalline structure by $^2H-^{13}C$ 2D HMQC spectroscopy, applied to an α-hydrogen-deuterated and $^{13}C{\equiv}N$-labeled aPAN sample. The large quadrupolar interactions of the deuterons and the large CSA widths of the $^{13}C{\equiv}N$ carbons provide good angular resolution in the NMR experiments, and the well-defined electric field gradient and chemical shift tensor orientations, respectively, have enabled us to determine torsion angles accurately. The successive average torsion angles and their distributions in racemo trans–trans dyads have been deter-

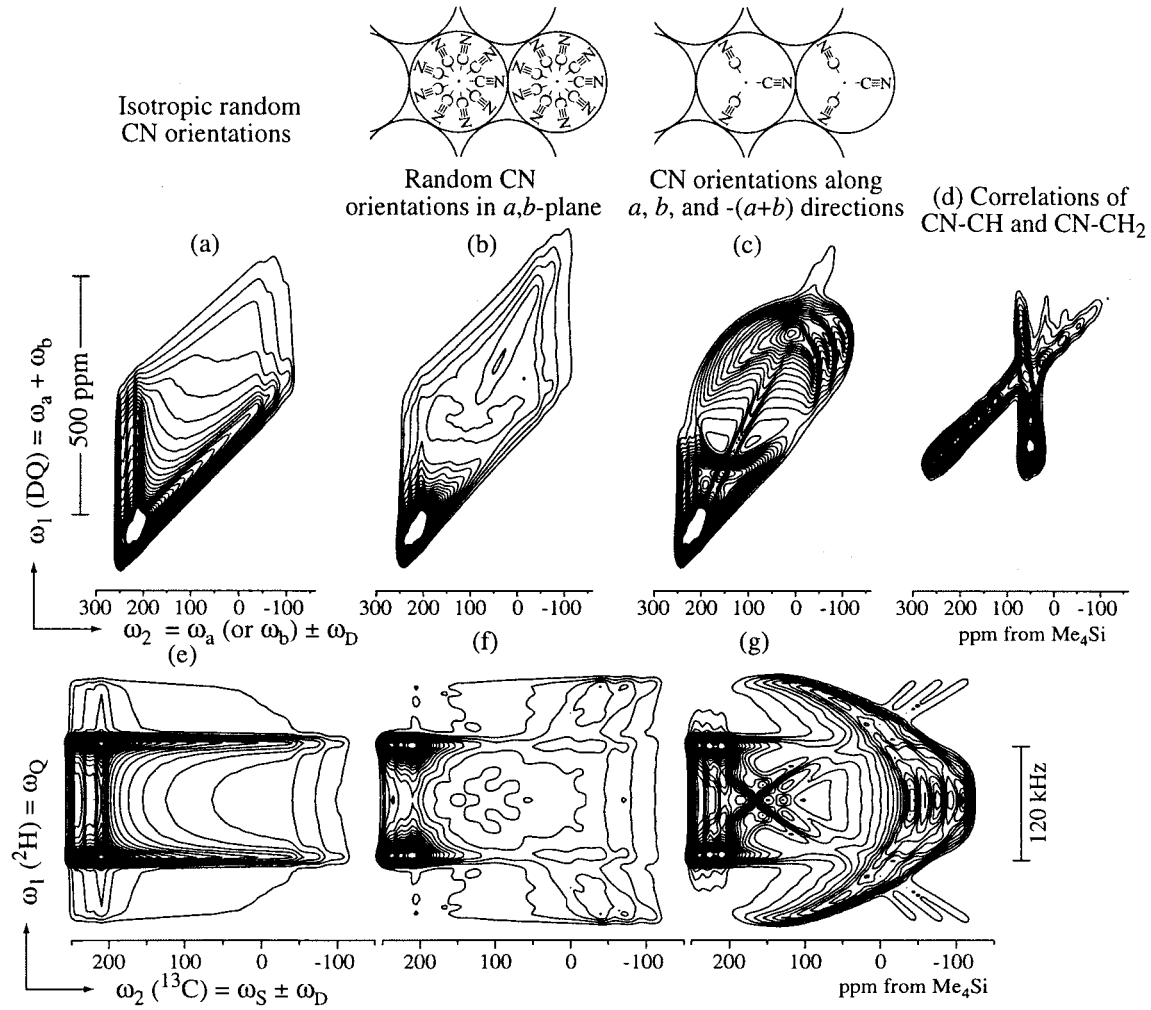

Figure 6. (a−c) Simulated 2D DOQSY spectra of ^{13}CN-aPAN with intermolecular ^{13}CN−^{13}CN correlations: (a) isotropic random C≡N orientations, (b) random C≡N orientations in the *a*,*b*-plane, (c) C≡N orientations along the *a*, *b*, and −(*a* + *b*) directions. (d) Simulated 2D DOQSY spectra of ^{13}CN-aPAN with correlations between ^{13}C≡N and natural-abundance aliphatic carbons. Thirty contour lines are plotted between 2% and 60% and between 3% and 90% of the maximum intensity for (a)−(c) and (d), respectively. Other parameters are the same as in Figure 5 of ref 2. (e−g) Simulated ^{2}H−^{13}C 2D HMQC spectra of ^{2}H/^{13}CN-aPAN with the same intermolecular ^{2}H−^{13}CN correlations as shown in (a)−(c), respectively. Thirty contour lines are plotted between 3% and 90% of the maximum intensity. Other parameters are the same as in Figure 3. In (b), (c), (f), and (g), no translational distributions along the chain direction have been included.

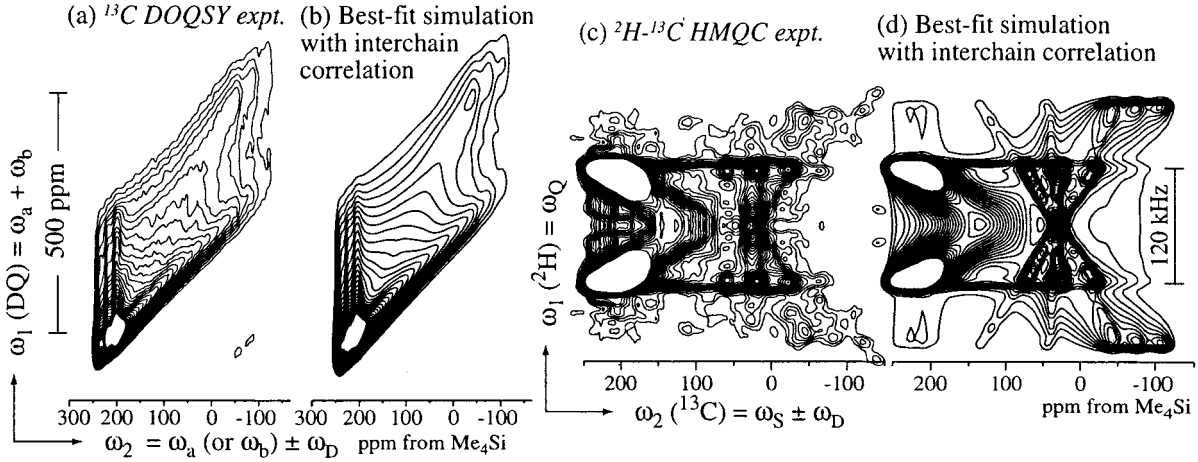

Figure 7. Comparison of experimental spectra with fits combining intra- and intermolecular correlations. (a) Experimental ^{13}C DOQSY spectrum. (b) Best-fit DOQSY simulation with an intermolecular correlation contribution of 7% of the integrated intensity, from CN groups pointing along the *a*, *b*, and −(*a* + *b*) directions in the crystalline lattice. (c) Experimental ^{2}H−^{13}C HMQC spectrum. (d) Best fit ^{2}H−^{13}C HMQC simulation with 3% of the intermolecular correlation component, with the geometry described in (b).

mined to be (180 ± 5°, 180 ± 5°) with standard deviations of $\sigma = 10 \pm 5°$. From our previous 2D DOQSY experiments, the successive torsion angles in meso trans−trans dyads were determined to deviate from

180° trans on average by 10−20°, and to be broadly distributed with $\sigma = 20 \pm 5°$. The trans:gauche ratio was also measured to be 90:10 (±5%). These $^2H-^{13}C$ HMQC and ^{13}C DOQSY experiments are the first quantitative measurements of the torsion angle deviations from the ideal trans state in meso trans−trans dyads in aPAN and of the torsion angle distributions in both meso and racemo dyads. A clear difference in torsion angles of meso and racemo dyads has been detected, which originates from large steric and electrostatic interaction between CN groups in meso trans−trans dyads. The torsion angle distributions in meso and even racemo dyads permit the polymers to form cylindrical chains that can pack in the pseudohexagonal (or orthorhombic) structure determined by X-ray diffraction.

Semiquantitative information on intermolecular alignments has also been obtained by detailed analyses of 2D DOQSY spectrum. Analysis of the specific misfit between the experimental and best-fit intramolecular simulated spectra suggests that the $^{13}C\equiv N$ side groups are mostly oriented along the crystalline lattice directions a, b, and $-(a + b)$ in the hexagonal lattice. Intermolecular antiparallel alignment of C≡N groups, which is often found in organic nitrile compounds, has not been observed in our NMR experiments on aPAN samples.

The combinations of advanced solid-state NMR techniques and suitable isotopic labeling presented in this series of papers make it possible to obtain precise conformational information for meso and racemo dyads selectively, although they are statistically mixed along the polymer chains. Not only a single angle but two successive torsion angles can be obtained by these experiments; this is indispensable information for characterizing the local chain conformation. Similar approaches will open the way for detailed, quantitative structural characterizations of various complex materials with heterogeneous nanometer-scale structures.

Acknowledgment. H.K. thanks the International Fellowship by the Ministry of Education, Science, Sports and Culture, Japan, for financial support. K.S.R. thanks the National Science Foundation (Grant DMR 9703916) for funding this work and NSF/MRSEC for support of the NMR facility.

References and Notes

(1) Kaji, H.; Schmidt-Rohr, K. *Macromolecules* **2000**, *33*, 5169.
(2) Kaji, H.; Schmidt-Rohr, K. *Macromolecules* **2001**, *34*, 7368.
(3) Schmidt-Rohr, K.; Hu, W.; Zumbulyadis, N. *Science* **1998**, *280*, 714.
(4) Dunbar, M. G.; Novak, B. M.; Schmidt-Rohr, K. *Solid State Nucl. Magn. Reson.* **1998**, *12*, 119.
(5) Schmidt-Rohr, K. *Macromolecules* **1996**, *29*, 3975.
(6) See references in ref 1.
(7) Schmidt-Rohr, K.; Spiess, H. W. *Multidimensional Solid-State NMR and Polymers*; Academic Press: London, 1994.
(8) Bax, A.; Griffey, R. H.; Hawkins, B. L. *J. Magn. Reson.* **1983**, *55*, 301.
(9) Muller, L. *J. Am. Chem. Soc.* **1979**, *101*, 4481.
(10) Dunbar, M. G.; Sandström, D.; Schmidt-Rohr, K. *Macromolecules* **2000**, *33*, 6017.
(11) Siminovitch, D. J.; Griffin, R. G. *J. Magn. Reson.* **1985**, *62*, 99.
(12) Henrichs, P. M.; Hewitt, J. M.; Linder, M. *J. Magn. Reson.* **1984**, *60*, 280.
(13) Liu, X. D.; Ruland, W. *Macromolecules* **1993**, *26*, 3030.
(14) Hobson, R. J.; Windle, A. H. *Polymer* **1993**, *34*, 3582.
(15) Chatani, Y.; Maruyama, H.; Noguchi, K.; Asanuma, T.; Shiomura, T. *J. Polym. Sci., Part C: Polym. Lett.* **1990**, *28*, 393.
(16) Rizzo, P.; Auriemma, F.; Guerra, G.; Petraccone, V.; Corradini, P. *Macromolecules* **1996**, *29*, 8852.
(17) Wunderlich, B.; Grebowicz, J. *Liquid Crystalline Polymers II/III*; Springer-Verlag: Berlin, 1984; Vol. 60/61.
(18) Wunderlich, B.; Moller, M.; Grebowicz, J.; Baur, H. *Conformational Motion and Disorder in Low and High Molecular Mass Crystals*; Springer-Verlag: Berlin, 1988; Vol. 87.
(19) *Handbook of Chemistry and Physics*, 57th ed.; CRC Press: Boca Raton, FL, 1976.
(20) Saum, A. M. *J. Polym. Sci.* **1960**, *42*, 57.
(21) Bruckingham, A. D.; Raab, R. E. *J. Chem. Soc.* **1961**, 5511.
(22) Freedman, T. B.; Nixon, E. R. *Specrochim. Acta* **1972**, *28A*, 1375.
(23) Paoloni, L.; Hauser, S. *Bull. Soc. Chim. Belg.* **1975**, *84*, 219.
(24) Dagnino, M. R.; La Manna, G.; Paoloni, L. *Chem. Phys. Lett.* **1976**, *39*, 552.

MA010658C